Available online at www.sciencedirect.com
SCIENCE DIRECT®
Biomaterials 25 (2004) 4955–4962
Biomaterials
www.elsevier.com/locate/biomaterials

Biodegradable composite scaffolds with an interconnected spherical network for bone tissue engineering

Kārlis A. Gross*, Luis M. Rodríguez-Lorenzo

School of Physics and Materials Engineering, Monash University, Building 69, Monash University, 69, VIC 3800, Australia

Received 2 January 2004; accepted 20 January 2004

Abstract

Tissue engineering scaffolds are highly engineered structures that accommodate cells, facilitate their expression, and resorb to facilitate regeneration of tissue. A new technique for producing controlled pore shape and pore size interconnectivity offers promise for application as a tissue engineering scaffold. Salt particles were spheroidized in a flame and sintered to provide an interconnecting salt template. The salt template was filled with a carbonated fluorapatite powder and a polylactic polymer to produce a composite scaffold. It was found that a higher pore space is possible with the use of spherical and larger salt particle sizes. This technique can produce scaffolds with good interconnectivity and be suitable for producing pore size graded bodies.

Keywords: Scaffold architecture; Template; Pore connectivity; Pore shape; Salt leaching; Bone tissue scaffold

1. Introduction

Tissue engineering, the use of living cells together with either natural or synthetic extracellular components for implantable components and devices [1] is continually being developed to meet the increasing demand for tissue and organ substitutes. The disadvantage of autografts and allografts [2–4] and the shortage of donors has placed emphasis on synthetic means of reconstructing tissue and organs [5]. This process relies on the correct selection of bioresorbable materials in concert with a cell culture that together can produce a suitable biological tissue for implantation. Growth of a tissue or organ requires a cell culture seeded onto a support for cell growth and differentiation. This may be initiated outside the body, in a bioreactor or by the implantation of a porous scaffold inside the body. These cell-populated structures are not immediately functional and cannot immediately restore the vital functions of the implantable site in the body. Filling of the scaffold with a new tissue and the resorption speed of the scaffold must be balanced to provide the optimum tissue formation conditions.

The growth of tissue engineering has provided a platform for introducing a highly engineered pore network in established biomaterials to form scaffolds. Certain characteristics were established early from the use of porous biomaterials as a means of fixation. Pores needed to be greater than 100 μm for bone tissue ingrowth [6]. Studies on corals revealed that pore connectivity was necessary for deeper tissue growth within the porous body [7]. These channels allowed the supply of oxygen and nutrients to cells inside the scaffold and facilitated waste transfer out of the scaffold. The requirement of pore size and connectivity were thus quickly established for scaffolds.

Tissue growth will be implant site specific, dictated by the growth conditions, and also by the type of tissue being regenerated. The speed of tissue growth can be greatly influenced by biomaterial factors. A biomaterial must resorb at a sufficiently high rate to accommodate the new tissue. Tissue growth will be implant site specific, dictated by the growth conditions, and also by the type of tissue being regenerated. The degradation products may further influence cell differentiation and health and thus a good knowledge of the degradation products is essential for selection of biomaterials in scaffold applications. Unlike other implants, where the degradation products may be removed by the surrounding fluid flow, the pore network within a scaffold cannot

*Corresponding author. Tel.: +61-3-9905-4910; fax: +61-3-9905-4940.
E-mail address: karlis.gross@spme.monash.edu.au (K.A. Gross).

0142-9612/$ - see front matter © 2004 Elsevier Ltd. All rights reserved.
doi:10.1016/j.biomaterials.2004.01.046

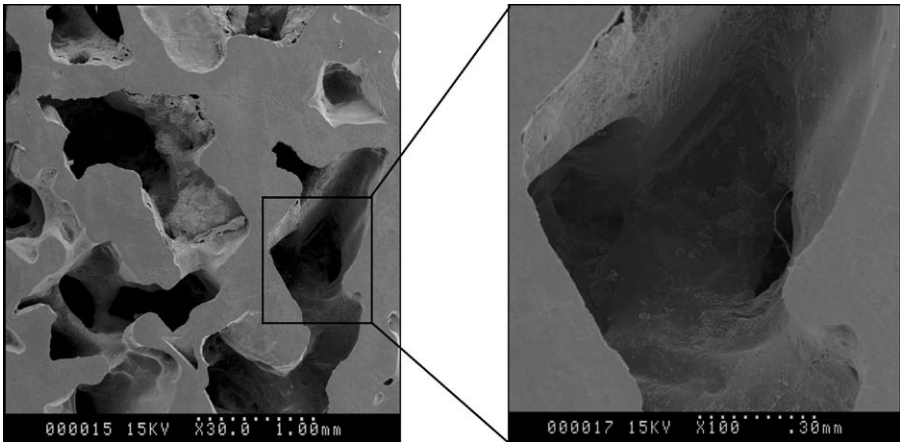

Fig. 1. Scaffold from a template made from angular salt particles.

offer as high a fluid exchange and thus cells are expected to be more sensitive to the degradation products of biodegradable scaffold materials. Calcium phosphates dissolve to produce phosphate and calcium, both of which are widely distributed in the body, needed for cellular function, and are thus suitable for use in scaffolds [8]. The brittle nature of calcium phosphates can be overcome by incorporating the calcium phosphates with polymeric materials, analogous to the composite nature of bone.

The physical characteristics of a scaffold can be described by an average pore size, the pore size distribution, pore volume, pore interconnectivity, pore shape, pore throat size and pore roughness. A minimum pore size is required for tissue growth [9], interconnectivity for access to nutrients and transport of waster products, pore shape and roughness for better cell spreading [10] and pore throat size for passage of tissue throughout the scaffold. The physical aspects of scaffolds are typically dictated by the choice of manufacturing process. Placement of different chemical compounds or growth factors within the scaffold walls or adsorbed to the pore walls can further enrich the scaffold to promote cellular behaviour or tissue growth [11].

The range of scaffold manufacturing techniques is the most diverse for polymers covering the use of porogens, chemical segregation [12] and rapid prototyping [13]. Porogens represent a common approach for introducing porosity with freeze drying, salt leaching or dissolution of salt templates. Isolated ice particles are joined as sublimation provides pore interconnectivity. Salt leaching is limited to polymers, due to the low interconnectivity of particles randomly assembled in a biopolymer dissolved with a solvent. Pores are dictated by the salt particles and are typically angular. Chemical segregation offers the ability to control the pore morphology as one phase is removed with a solvent. Rapid prototyping, including processes such as fused deposition modelling, selective laser sintering, stereolithography and three-dimensional printing, are able to control the pore size and interconnectivity very effectively, but cannot control other aspects such as pore shape and roughness. All the above-mentioned techniques are capable of producing scaffolds and are very often used in conjunction with another technique to enhance the pore characteristics.

Salt leaching is a very simple approach but is limited in the control of pore shape and connectivity. Initial work revealed limited pore interconnectivity produced with loosely packed salt particles [14]. The low probability of pore interconnectivity limited the scaffold size to a thickness of 3 mm. This limitation was overcome by producing interparticle connections that has been possible by placement of the salt particle arrangement in a humid atmosphere [15] or by sintering [16,17]. The resulting polymeric scaffold that can be formed from the connected salt template is illustrated in Fig. 1. An enlarged view illustrates connecting channels at the base of a pore, with adjacent pores. The purpose of this work is to investigate the use of spherical salt particles to produce templates with an improved pore shape, good pore interconnectivity, reproducible pore throat size that can be used for producing a load bearing composite scaffold for cell seeding in bone tissue engineering applications.

2. Materials and methods

2.1. Apatite synthesis

Carbonated fluorapatite with the composition of $Ca_{9.223}Na_{0.518}(PO_4)_{5.223}(CO_3)_{0.777}F_{1.741}$ was synthesized by adding di-ammonium hydrogen phosphate with sodium bicarbonate and sodium fluoride at a rate of 10 ml/min into a calcium nitrate solution at 37°C. The pH in the calcium solution was adjusted to 9.4 with a pH

stat (Titrino 736, Metrohm, Switzerland) after which addition of the phosphate solution commenced. During the reaction, the pH was continuously adjusted to 9.4 to ensure constant pH conditions during the synthesis. The obtained powder was filtered, washed, dispersed in ethanol and dried for 12 h at 104°C. The powders were then calcined using a heating rate of 10°C/min until 500°C and then maintained at temperature for 2 h. The characteristics of this powder are available elsewhere. X-ray diffraction (XRD) patterns were collected from $10-2\theta$ to $90-2\theta$ using a Rigaku Geigerflex diffractometer with Bragg–Bentano geometry in a step mode with a step size of 0.02° and 10 s per step using Copper Kα radiation at 40 kV and 22.5 mA passing through a 0.5° divergence slit and 0.3° receiver slit.

Crystal size and lattice strain were calculated for (0 0 1) direction, using the Scherrer equation [16]. The formulae used for the calculations are:

$$\text{Crystallite size } C_s \equiv \frac{K \times \lambda}{W_{size} \times \cos\theta} \text{with } W_{size} = W_b - W_s,$$

$$\text{Lattice strain } L_s \equiv \frac{W_{strain}}{4\tan\theta} \text{with } W_{strain} = (W_b^2 - W_s^2)^{1/2},$$

where K is the form factor assumed to be 0.9, λ wavelength, W_{size} is the broadening caused by small crystals, W_b is the broadened profile width, W_s is the standard profile width and W_{strain} is the broadening caused by lattice distortion.

2.2. Salt particle preparation

Sodium chloride rock salt with a mean size of 2 mm was ball milled for 1 min at 300 rpm in an alumina vessel and then sieved with a vibratory stack of sieves for 60 min to obtain powder within particle size ranges of <100, 100–150, 150–300, 300–500 and >500 μm. Salt was then dried in an oven at 120°C to remove any adsorbed moisture and facilitate particle packing when placed in a measuring cylinder to measure the packing volume. The salt weight and occupied volume were then used to determine the packing efficiency.

Salt was spheroidized by external injection into a Metco 5P (Sulzer Metco, Wohlen, Switzerland) flame spray torch at a rate of 1 g/min to optimize the heat transfer to the salt particles. Previous work has indicated that particles smaller than 150 mm are spheroidized effectively when the torch is used in the conventional manner [17]. Spheroidization of larger particles was investigated by increasing the dwell time and decreasing the particle velocity within the flame.

2.3. Template manufacture

Ten grams of sieved salt particles of different size ranges were placed in a 20 mm diameter alumina crucible for sintering. Sodium chloride spherical particles were sintered in a muffle furnace for 2 h. These salt templates were examined by scanning electron microscopy in a Hitachi S570 (Tokyo, Japan).

The packing density was assessed for particles and the sintered template. The packing density for particles was assessed by pouring particles into a measuring cylinder to fill a volume of 20 ml^3 and then weighing the powder needed to fill this volume. The salt assembly was placed on a vibratory base for 1 min to maximize particle packing. Template volume was determined by weighing the cylindrical pellet and then determining the dimensions of the pellet for a calculation of the density.

To assess the continuity of the salt network, epoxy resin was mounted into the porous salt block using vacuum impregnation. The epoxy was ground, and the salt dissolved in water to reveal the pore network in a scanning electron microscope.

2.4. Scaffold production

A suspension of 17 g of apatite in 25 ml of pure ethanol was prepared with mechanical and ultrasonic agitation. Sodium chloride templates were soaked twice for 5 min in the apatite suspension while resident in an ultrasonic bath. The sodium chloride template with the apatite slurry was dried in an oven at 100°C for 3 h.

Poly(L-lactic acid), a weight of 0.2 g, was dissolved in 6 ml of CH_3Cl and introduced into the apatite filled salt template by pouring over the template. The solvent was allowed to evaporate at room temperature for 24 h and then in vacuum at −100 kPa for an additional 24 h.

The 18 mm high template filled with apatite and polylactic acid was soaked in deionized water for 30 min to remove the interconnected salt template. After drying, the scaffold was fractured and examined in the scanning electron microscope.

3. Results

The yield from the milling and sieving operation provided 30% of the particles between 150 and 300 μm and another 30% larger than 300 μm, Fig. 2. Previous investigations have indicated that particles smaller than 150 μm can be spheroidized effectively when the torch is used in the conventional manner [17]. Spheroidization of larger particles required the optimization of the spray conditions by increasing the dwell time and decreasing the particle velocity within the flame.

The flowability of salt particles changed with particle size exhibiting a decrease with smaller particle size. The

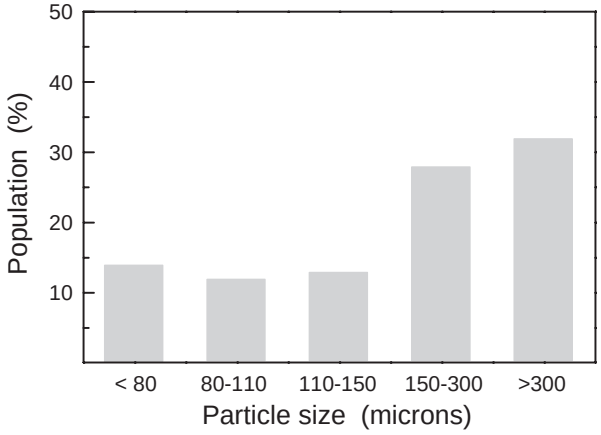

Fig. 2. Salt particle size distribution after communition.

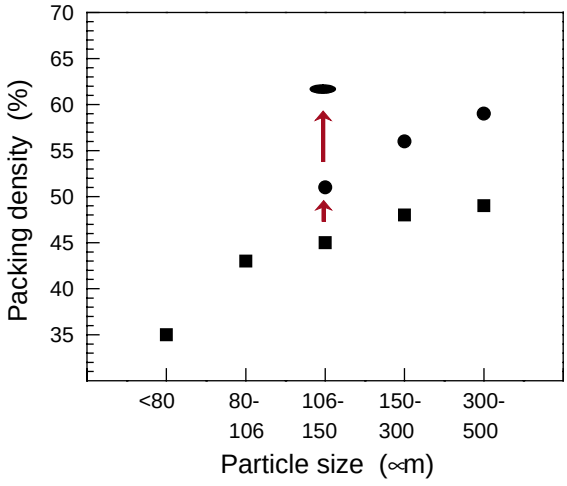

Fig. 3. Particle packing of angular, spheroidized and sintered particles with a different size range.

poor flowability of smaller particles was accentuated with time as moisture was readily adsorbed onto the particle surface. Salt particles were initially dried in an oven to minimize the adsorbed moisture.

Particles less than 80 μm produced a packing density of 35%, Fig. 3. This increased significantly to 43% with the next particle size range (80–106 μm). Larger particle size ranges only provided a small improvement in the packing, reaching a value of 48% for 300–500 μm particles.

Spherical particles produced by thermal spraying provided an increase in the packing density. A 5% increase was noted for salt particles in the 106–150 μm range. The improvement in the packing density increased with particle size and reached a value of 59% for the 300–500 μm particle size range. Sintering of the particle compact led to another increase in packing density, reaching a value of 62% for the 106–150 μm salt particles.

Salt particles sintered for 2 h produced a salt compact that could be handled with ease without causing fragmentation. The template could be removed from the alumina crucibles in a cylindrical form. A fracture surface was formed from the sintered salt template to investigate the connectivity, and it was found that particles established a sound bond with surrounding particles placed in relative contact from the powder filling of the alumina crucibles, Fig. 4. The surface view of the 150–300 μm salt particles revealed underlying interconnected particles and a fracture surface which displayed good interconnectivity. Similarly, larger particles also exhibited good interconnectivity and the fracture revealed failure in the throat areas more commonly than through the core of the particle, Fig. 4b. Throat areas in the template made from salt particles larger than 500 μm were still observed, despite the more irregular packing provided by rounded particles that exhibited rough areas from the unmolten areas of particles.

The throat size/neck size produced between the separate salt particles exhibited an increase with particle size, Fig. 5. The neck size increased from 60 ± 5 μm for 106–150 μm particles to 90 ± 8 μm for 300–500 μm particles. This corresponds to a ratio of particle size to neck size of 3.8, 5 and 5.1 for the increasing particle size ranges. A large difference is apparent between the smaller particle sizes, but the small change with particles greater than 500 μm could be attributed to the rounded but non-spherical shape of the salt particles that did not facilitate good particle contact. The particle contact for well-packed particles clearly provides areas of a negative and positive curvature that act as sites for vaporized material deposition and removal.

The carbonated fluorapatite, consists of small crystallites with a crystal size of 326 A and a 64% crystal strain in the (0 0 1) direction resembling francolite. The small crystallites could readily fill the large pore spaces within the sintered salt template. Dispersion of the apatite in chloroform did not lead to any noticeable dissolution. This provided good transfer of the apatite particles into the pore space of the salt template. Drying of the filled salt template in an oven for 1 day ensured good solvent removal.

Chloroform as a solvent was chosen on the basis of readily dissolving the polylactic acid, not dissolving the apatite crystallites and the salt template. Separately drying the apatite filled scaffold followed by drying of the polylactic acid decreased the amount of solvent that could remain in the scaffold.

Pouring the dissolved polylactic acid over the apatite filled salt template filled the pore space and the area surrounding the scaffold. The outer layer of the template was covered with a layer of apatite crystallites, and this remained on the surface of the scaffold, bound with the polylactic acid. This is observed as the fine-grained area on the right side of Fig. 6a. The polylactic acid that has penetrated into the pore space of

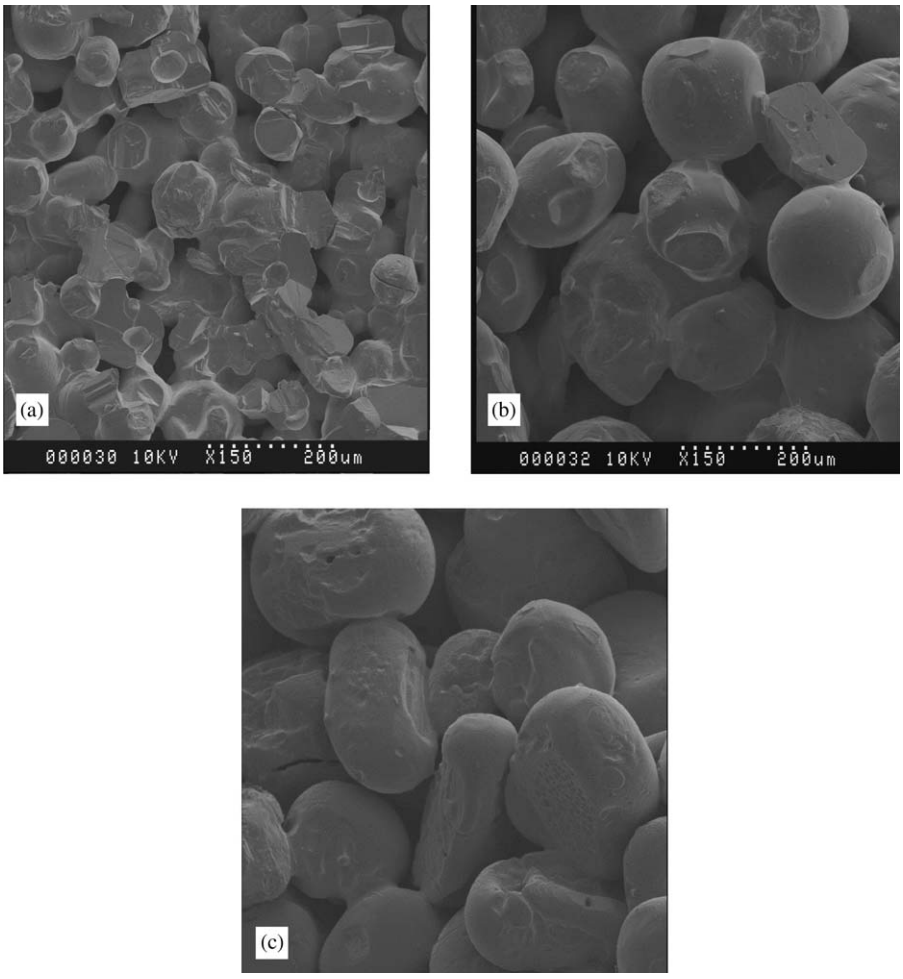

Fig. 4. Salt template consisting of (a) spherical 150–300 μm particles, (b) spherical 300–500 μm particles and (c) rounded >500 μm particles.

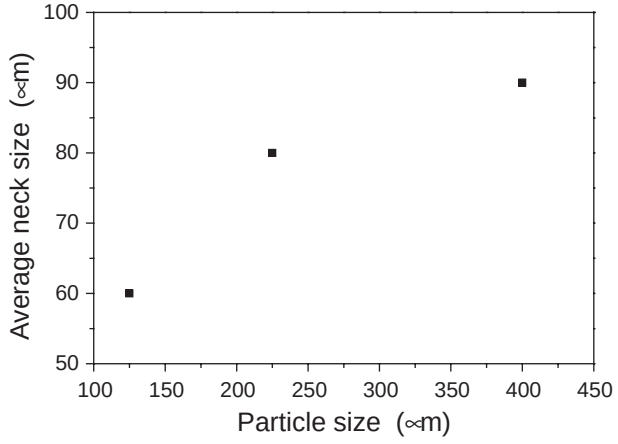

Fig. 5. Neck size of sintered salt particles of different particle sizes.

the salt template filled the pore space to produce a scaffold structure. Higher magnification of the pore walls revealed that fine pores remained within the walls, and the polylactic acid exhibited a tendency to fill the space between the agglomerated apatite deposit and the salt template. This produced a structure of loosely agglomerated apatite crystals within the pore walls, which was sealed with a layer of polylactic acid. The same distribution of the polylactic acid and apatite was observed with the template that contained a larger pore space, Figs. 6b and c.

4. Discussion

The pore space characteristics offered by the salt template are unique and different from other scaffold manufacturing processes. Sintering salt particles has produced an interconnected spherical pore network in the scaffold with the ability to control the throat size and pore wall characteristics.

The throat size is a function of the sintering conditions, a longer sintering time producing a larger throat size, and thus providing a template with larger interconnecting regions. This can produce a scaffold with less fluid flow resistance, that can be an advantage when filling the template during the scaffold manufacture

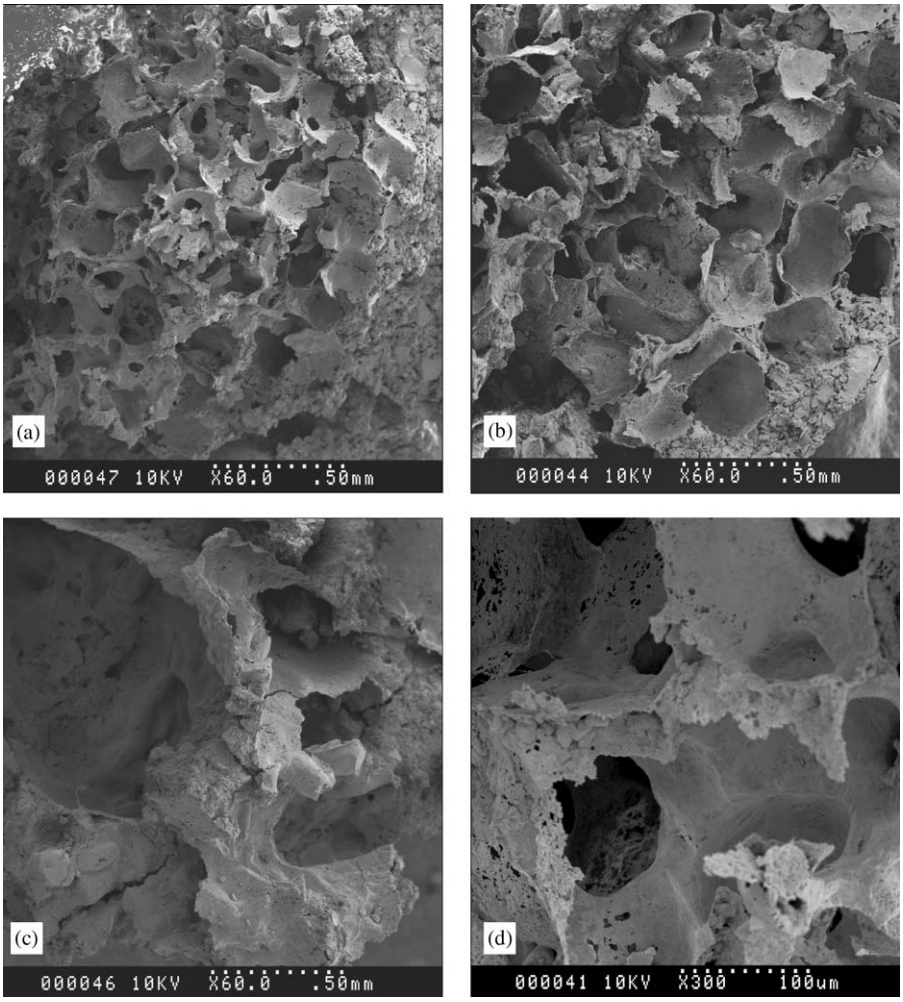

Fig. 6. PLLA reinforced apatite scaffolds manufactured from scaffolds using (a) 150–300 μm salt particles, (b) 300–500 μm salt particles and (c) > 500 μm salt particles. An enlarged view of (a) is shown in (d).

but also for easier stem cell placement and improved fluid transport throughout the scaffold when implanted in the body.

The time for establishing the sintered necks was significantly lower than that required for sintering angular particles. This is attributed to the stress condition within the spherical salt particles compared to the angular particles. Small salt particles are completely molten, whereas larger salt particles are only molten in the outside shell. Solidification will commence from the outside for the smaller particles, but from the core of partially molten larger particles. The shell on smaller molten droplets solidifies first and creates a rigid surface for further solidification. The contraction from the liquid to solid leads to the presence of voids within the spheres, but also places the shell in a compressive residual stress condition. Larger particles will have the shell in a tensile residual stress condition as the molten shell solidifies. These residual stress conditions provide stored energy that hastens the sintering process compared to angular particles. The observation of a larger throat size in the larger particles could be attributed to a higher stress condition in the solidified salt particles.

Salt particles experience very little densification attributed to the evaporation–condensation process as the governing sintering mechanism within halides [18]. The amount of densification decreases 10-fold from 20% for 38 μm particles to 1% for 100 μm particles under the same sintering conditions [19]. The 20% improvement in the packing density could thus be explained by the other sintering mechanisms playing a more important role in the sintering of thermally sprayed particles. This is thought to arise from the higher ionic mobility within the salt structure attributed to the high defect concentration that is characteristic for rapidly solidified materials. The use of longer sintering times is expected to be a good means of increasing the salt packing density to values higher than 62%. The longer sintering time would be expected to produce wider throat sizes and higher packing densities. This is an advantage in those situations where mechanical loads

do not need to be supported, allowing the use of a higher pore content scaffold.

A unique surface feature that occurs as a result of the evaporation–condensation sintering mechanism is the appearance of ledges surrounding the point of low curvature [16]. Given that the surface profile is reproduced in the scaffold, these fine ledges can be used to an advantage for tissue guidance and provide a surface for good cell attachment. It has previously been shown that fine grooves can be useful for controlling the direction of cellular migration over a surface [20] and can be used for faster filling of the interior scaffold surface. Since a surface with roughness is important for cell expression, the combination of a roughness and directional ridges can be important aspects for controlling the speed of cell guidance and resulting tissue growth with the scaffold. The spherical pore shape will act as the ideal surface for the ridges by providing a surface for ease of cell spreading, unlike an angular pore that will suspend cell movement within the scaffold.

This technique has shown that salt leaching is no longer limited by a 3 mm thick scaffold as previously set by Mikos [14]. Interconnected pore networks can be manufactured to any desired scaffold size sintering an assembly of salt spheres. Sintered angular particles produce a low packing density, a broad range in pore throat size and thus an inhomogeneous distribution of similar pore throat sizes within the scaffold. This is a result from the wide range of particle assembly configurations, Fig. 7. The largest throat size can be produced when the face of one angular particle resides adjacent to another particle, however the chances of this configuration are very low in comparison to a particle corner abutting onto the corner, side or face of another particle. The use of angular particles is not a sound means of producing a uniform throat size throughout the scaffold. This can only be established with the use of spherical salt particles that will also exhibit a better packing efficiency.

Other scaffold manufacturing approaches may be used in parallel with the described technique. The use of two approaches in conjunction has been used previously to increase the amount of open porosity within a scaffold, or to lead to a stiffer scaffold. Previous studies have shown than sections up to 300 μm may be stiffened using the gas foaming technique [21]. This is an ideal technique for increasing the stiffness of such scaffolds to be suitable for load bearing sites within the body. The pore walls can also be modified using a spinodal decomposition technique to introduce small pores between the larger pore spaces in the final scaffold [22]. These techniques when used in conjunction can tailor the pore architecture and material properties for enhanced performance. Other polymeric materials that are readily dissolved in a solvent such as chloroform can be used in this technique.

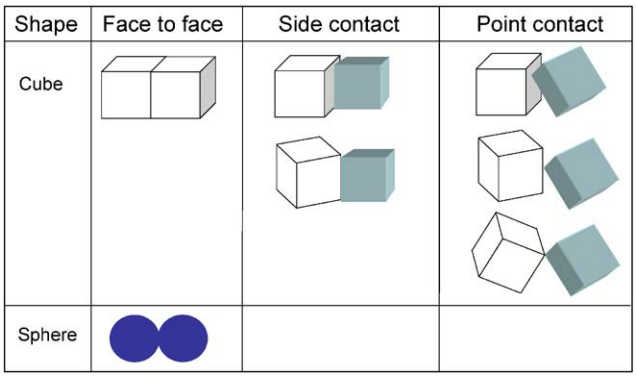

Fig. 7. Influence of particle shape on the neck characteristics.

An attractive feature of this process is the ability to shape the salt template to the required geometry for implantation in the body. The sintered form can be easily ground to the desired shape. The internal pore architecture can be well controlled to produce a spherical pore shape, a desired pore size, pore throat size, and pore roughness. A graded pore structure and the inclusion of larger channels can be easily manufactured by assembly salt particles of different sizes. This innovative process provides control over a range of features that is not commonly available within scaffolds and offers great potential for bone tissue engineering where the scaffold strength and stiffness and strength can be further tailored with a composite and pore wall pore structure control.

5. Conclusion

Production of a salt template from spherical salt particles is a novel technique that offers pore interconnectivity, pore shape control, throat size design for scaffolds to be used in bone tissue engineering applications. It was found that spherical particles provide a higher pore volume scaffold than angular particles and can offer a more homogeneous pore size distribution throughout the scaffold.

Acknowledgements

This work was supported by the Australian Research Council with grant F10017027 and the Monash Research Fund.

References

[1] Patrick CW, Mikos AG, McIntire LV. Frontiers in tissue engineering. Oxford: Pergamon Press; 1998.

[2] Smet HT. Tissue transfers in reconstructive surgery. New York: Raven Press; 1989.
[3] Bucholz RW. Nonallograft osteoconductive bone graft substitutes. Clin Orthop Rel Res 2002;395:44–52.
[4] Delloyle C, Cnockaert N, Cornu O. Bone substitutes in 2003: an overview. Acta Orthop Belg 2003;69(1):1–8.
[5] Davies JE. Bone engineering. Toronto: Em Squared Inc; 2000.
[6] Ravaglioli A, Krajewski A. Bioceramics and the human body. Dordrecht: Kluwer Academic Publisher; 1992.
[7] Guillemin G, Meunier A, Dallant P, Christel P, Pouliquen JC, Sedel L. Comparison of coral resorption and bone apposition with two natural corals of different porosities. J Biomed Mater Res 1989;23(7):765–79.
[8] Gross KA, Berndt CC. Biomedical application of apatites. In: Kohn MJ, Rakovan J, Hughes JM, editors. Phosphates: geochemical, geobiological and materials importance, vol. 48. Washington, DC: Mineralogical Society of America; 2003. p. 631–72.
[9] Zeltinger J, Sherwood JK, Graham DA, Mueller R, Griffith LG. Effect of pore size and void fraction on cellular adhesion, proliferation and matrix deposition. Tissue Eng 2001;7(5):557–72.
[10] Ranucci C, Moghe PV. Polymer substrate toography regulates the multicellular organization and liver-specific functions of cultured hepatocytes. Tissue Eng 1999;5:407–20.
[11] Gittens SA, Uludag H. Growth factor delivery for bone tissue engineering. J Drug Tragetting 2001;9(6):407–29.
[12] Nam YS, Park TG. Porous biodegradable polymeric scafffolds prepared by thermally induced phase separation. J Biomed Mater Res 1999;47:8–17.
[13] Chua CK, Leong KF, Cheah CM, Chua SW. Development of a tissue engineering scaffold structure library for rapid prototyping. Part 1: investigation and classification. Int J Adv Technol 2003; 21:291–301.
[14] Mikos AG, Thorsen AJ, Czerwonka LA, et al. Preparation and characterization of poly L-lactic acid foams. Polymer 1994;35:1068–74.
[15] Murphy WL, Dennis RG, Kileny JL, Mooney DJ. Salt fusion: an approach to improve pore interconnectivity within tissue engineering scaffolds. Tissue Eng 2002;8(1):43–52.
[16] Gross KA, Rodríguez-Lorenzo LM. Interconnected pore networks from sintered salt particles for scaffolds in tissue engineering applications. J Aust Ceram Soc 2003;39(1):35–9.
[17] Gross KA, Rodriguez-Lorenzo LM. Thermally sprayed scaffolds for tissue engineering applications. Key Eng Mater 2004; 254–256:961–4.
[18] Moser JB, Whitmore DH. Kinetics of sintering of sodium chloride in the presence of an inert gas. J Appl Phys 1960;31(3): 488–93.
[19] Thompson RJ, Munir ZA. Influence of particle size on the sintering kinetics of ultrapure sodium chloride. J Am Ceram Soc 1982;65(6):312–6.
[20] Chen CS, Mrksich M, Huang S, Whitesides GM, Ingber DE. Micropatterned surfaced for control of cell shape, position and function. Biotechnol Progr 1998;14(3):356–63.
[21] Nam YS, Yoon JJ, Park TG. A novel fabrication method of macroporous biodegradable polymer scaffolds using gas foaming salt as a porogen additive. J Biomed Mater Res 2000; 53:1–7.
[22] Cai Q, Yang J, Bei J, Wang S. A novel porous cell scaffold made of polylactide-dextran by combining phase-seperation and particle leaching techniques. Biomaterials 2002;23:4483–92.